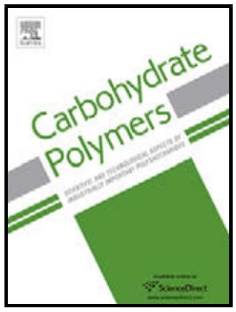

Title: Novel Route for Amine Grafting to Chitosan Electrospun Nanofibers Membrane for the Removal of Copper and Lead ions from aqueous medium

Authors: Sajjad Haider, Fekri A. Ahmed Ali, Adnan Haider, Waheed A. Al-Masry, Yousef Al-Zeghayer

PII: S0144-8617(18)30817-8
DOI: https://doi.org/10.1016/j.carbpol.2018.07.026
Reference: CARP 13826

To appear in:

Received date: 6-3-2018
Revised date: 28-6-2018
Accepted date: 9-7-2018

Please cite this article as: Haider S, Ali FAA, Haider A, Al-Masry WA, Al-Zeghayer Y, Novel Route for Amine Grafting to Chitosan Electrospun Nanofibers Membrane for the Removal of Copper and Lead ions from aqueous medium, *Carbohydrate Polymers* (2018), https://doi.org/10.1016/j.carbpol.2018.07.026

Novel Route for Amine Grafting to Chitosan Electrospun Nanofibers Membrane for the Removal of Copper and Lead ions from aqueous medium

Sajjad Haider*, Fekri A. Ahmed Ali, Adnan Haider, Waheed A. Al-Masry, Yousef Al-Zeghayer

Department of Chemical Engineering, college of Engineering, King Saud University, P.O. Box 800, Riyadh 11421 Saudi Arabia.

Highlights

- The study comprises of a novel route for the synthesis of amine grafted chitosan nanofibers (AGNFs) with potential as affinity membrane.
- The present systems showed enhanced adsorption capacity for Cu (II) on contrary to the already existing conventional adsorbents.
- 94% aqueous stability of the membrane enhanced its potential as more advanced water purification system.

Abstract

A novel step wise synthetic route was developed to prepare amine grafted nanofibers (AGNFs) affinity membrane. The chemical structure of the nanofibers (NFs) after grafting was studied by acquiring Fourier Transform Infrared (FT-IR) spectra and Carbon, Hydrogen and Nitrogen (CHN) data. The morphology of the NFs before and after grafting was studied by Field Emission Scanning Electron Microscope (FE-SEM). FT-IR and CHN data confirmed the introduction of new functional groups into the primary structure of chitosan (CH). FE-SEM showed denser membrane with no deterioration of the NFs morphology after grafting. The aqueous stability of the membranes was studied in distilled water. The AGNFs membranes showed good aqueous stabilities (with only ~ 6% loss in weight until 24 h and remained stable thereafter) which was less than the weight loss by glutaraldehyde treated nanofibers (GNFs) (~44% loss in weight until 24 h) and NFs (100% loss in weight as soon after it was immersed in distilled water). The maximum adsorption (q_m) capacity of AGNFs for Cu (II) and Pb (II) was observed to be 166.67 $mg.g^{-1}$ and 94.34 $mg.g^{-1}$. The adsorption capacity of the present systems was much higher for Cu (II) when compared to the already existing conventional and chitosan adsorbents. This increased might be related not just to the size, but more potentially to the increase in the number of nitrogen binding sites (chelating sites). Nitrogen donates lone-

pair of electron for chelation. The combination of processing and amine grafting (AG) significantly increased the adsorption capacity of NFs membranes.

Key words: Novel synthetic route; Chitosan nanofibers membrane; Improved aqueous stability; Bio-adsorbent; Enhanced metal ions removal

1. Introductions

NFs technology has enormously impacted both science and engineering disciplines. The motivations for the miniaturization process of polymers rest in producing nano-sized fibers with superior properties, e.g. high mechanical properties and large surface area per unit mass than micro fiber and film (Saeed et al., 2008). In addition to polymers functionalities (Saeed et al., 2008), the unique characteristics of NFs originated from being engineered in nanoscale and in different orientation have allowed NFs to be used in advance applications such as filtration, multifunctional membranes (Ma et al., 2005), composite reinforcement (Kim et al., 2005), tissue engineering scaffolds (Kotaki et al., 2005), wound dressings (Ueno et al., 2001), drug delivery (Katti et al., 2004), artificial organs (Huang et al., 2003) and vascular grafts, etc. NFs membranes fabricated from synthetic and biopolymers have received increased attention mainly due to the ease of fabrication and the ability to retain their compositional, structural and functional properties. The key advantage in producing fibers is stored in their extremely small diameters, large surface-to-volume ratio, high porosity and superior mechanical performance (Burger et al., 2006). Beside these advantages, the fabrication of NFs is greatly affected by the cost of the raw material. To minimize the raw materials cost without compromising on the desired properties. Recently, a number of the natural low-cost alternatives to synthetic polymers have been developed (Crini and Badot, 2008). Of late, the amply available natural biopolymers chitin, CH, gelatin, etc., have become cynosures due to their unusual combinations of properties, e.g. good biocompatibility, low toxicity, low immunogenicity, and mechanical and physical properties (Wang and Fu, 2009). However, applications of chitin are limited due to its

inherent insolubility and interactability. Gelatin on the other hand, though showed good solubility in acidic solvent, but it becomes unstable (readily get dissolve) in aqueous solution after processing and needs to be stabilized first to be used in the aqueous solution. CH ((1→4)-2-acetamido-2-deoxy-dglucan and (1→4)-2amino-2-deoxy-d-glucan) (Zhang et al., 2009; Md. R. A, 2015; Md. R. A et al., 2016; Md. R. A et al., 2015) an alkaline hydrolytic derivative of chitin has better solubility profile, less crystallinity and is open to chemical modifications due to the presence of functional groups such as hydroxyl, acetamido, and amine. The chemical modification of CH is of interest because modification would not change the fundamental skeleton of CH, would keep the original physicochemical and biochemical properties and finally would bring new or improved properties. Several chemical modifications such as oligomerization, alkylation, acylation, quternization, hydroxyalkylation, carboxyalkylation, thiolation, sulfation, phosphorylation, enzymatic modifications and graft copolymerization along with many assorted modifications have been carried out. The chemical modification affords a wide range of derivatives with modified properties for specific end user applications in diversified areas mainly of pharmaceutical, biomedical and biotechnological fields. Assorted modifications including CH hybrids with sugars, cyclodextrin, dendrimers and crown ethers have also emerged as an interesting multifunctional macromolecules. The versatility in possible modifications and the applications of CH derivatives presents a great challenge to scientific community and to industry. The successful acceptance of this challenge will change the role of CH from being a molecule in waiting to a lead player. CH has been investigated by several researchers as a biosorbent for the capturing of dissolved hazardous organic and inorganic materials from aqueous solutions (Mourya and Inamdar, 2008; Helder et al., 2007; Justus et al., 2004; Ngah et al., 2002; Bassi et al., 2000; Gupta, 1998; Huang et al., 1996; Gould and Genetelli 1978; Md, R. A et al., 2014; Md, R. A et al., 2018; Md, R. A et al., 2017; Md, R. A et al., 2017; Md, R. A et al., 2014; Md, R. A et al., 2014). Its use as a biosorbent is justified by two important advantages: firstly, its low cost compared to commercial activated carbon (CH is derived by

deacetylation of the naturally occurring biopolymer chitin, which is the second most abundant polysaccharide in the world after cellulose) and secondly, its outstanding chelation behavior (one of the major applications of this amino-polymer is based on its ability to tightly bind pollutants, in particular heavy metal ions and colored dyes) .

In the present work, experiments were performed to prepare chitosan NFs membrane by electrospinning process. After preparation, the membranes were grafted with diethylenetriamine (DETA) *via* a novel stepwise route and applied in a batch technique to synthetic solutions of copper (Cu(II)) and lead (Pb(II)) metals ions. In brief the NFs membranes were grafted by treating these with anhydrous potassium carbonate (K_2CO_3), glutaraldehyde (GTA) vapors, epichlorohydrin (ECH) and diethylenetriamine in step wise reactions.

2. Material and Methods

2.1. Material

Medium molecular weight CH powder, Trifluoroacetic acid (TFA (CF_3COOH)), DETA ($C_4H_{13}N_3$), sodium hydroxide (NaOH) were purchased from Sigma-Aldrich. ECH (C_3H_5ClO)), ethanol (C_2H_5OH) absolute and acetone (C_3H_6O) were purchased from Alfa Aesar, Paneac Quimica SAU and Scharlab S. L., respectively. Anhydrous potassium carbonate (K_2CO_3) and GTA ($C_5H_8O_2$) were purchased from Loba Chemie. All the chemicals were of analytical grade and were used without further purification. Distilled water was used for the preparation of K_2CO_3 solution. Teflon frame were prepared locally and were used to fix the edges of the NFs membrane to avoid shrinkage of the membrane during functionalization.

2.2. Preparation of CH NFs Membrane

To prepare the NFs membrane, 6 wt% CH solution was prepared by dissolving 0.6 g of CH powder into 10 mL of TFA. The solution was placed in sonicator bath (Model 2510) at 55 ^oC for 90 min to ensure complete dissolution of the CH. After dissolution, the solution was stirred

(Model Cerastir 30539) for 15 min and filtered using a mesh (with 0.063 mm pore size) to obtain homogeneous solution and remove any un-dissolved particles. The prepared CH solution was then added to a 5 mL plastic syringe and was electrospun at previously optimized conditions (Table 1) (Haider et al., 2012) using electrospinning machine (Model NANON-01A). The speed of the cylindrical collector was 100 rmp. The NFs membrane was removed from the aluminum foil, dried in the vacuum oven (Model ON-12) at 60 ^{o}C and -0.1 MPa and stored in the desiccator for functionalization. The experimental design used for the optimization of electrospinning conditions and preparation of the NFs membrane is shown in scheme1.

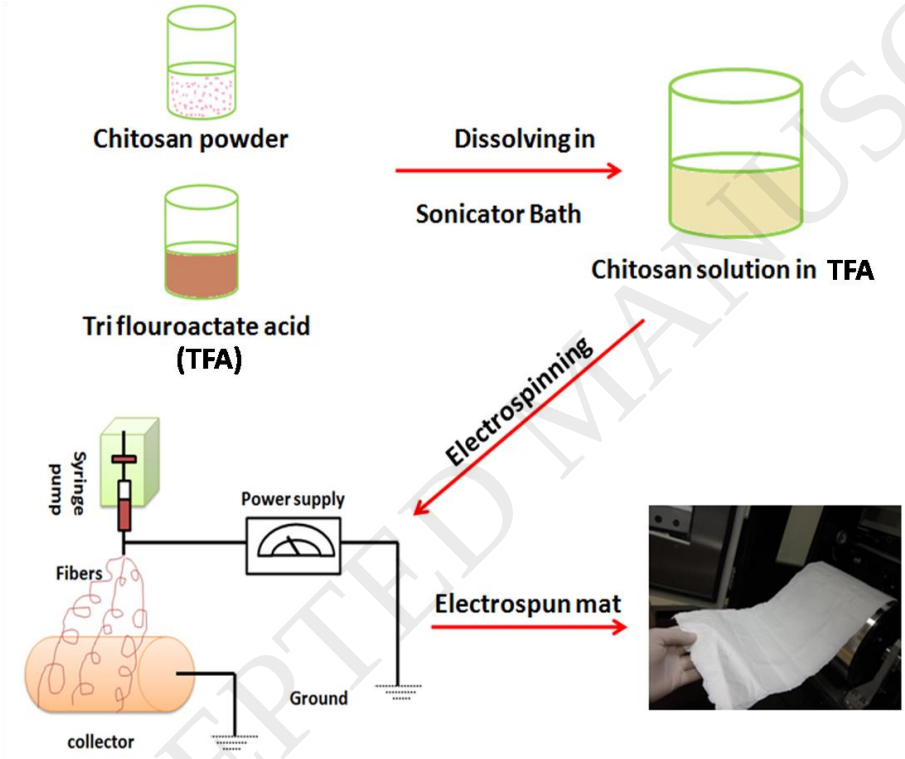

Scheme. 1. Experimental design used for the optimization of electrospinning conditions and preparation of the NFs membrane

Table 1. Optimal electrospinning parameters for the present system (Haider et al., 2012).

Parameter	Optimization value
Concentration Chitosan solution	6 wt%

Flow rate	ml/h 0.4
Voltage applied	kV 22
Needle diameter	mm 0.8
Distance between needle and collector	mm 100
diameter Nanofiber	nm 103

2.3. Step Wise Synthetic Route

2.3.1. Synthesis of GTA-CH NFs (GNFs) and GTA- neutralized-CH NFs (GNNFs) Membranes

The functionalization reaction of CH NFs membrane was carried *via* two steps. First the NFs membrane was placed on a porous ceramic shelf and 25% GTA aqueous solution in a dish at the bottom of the sealed desiccators at room temperature for 48 h. In the second step some of the membranes were rapidly transfer to a vessel containing $1M \cdot L^{-1}$ K_2CO_3 aqueous solution. The samples were allowed to remain in the vessel for 3 h at 25 ^oC. The membranes were named as GNFs and GNNFs, respectively. After reaction, the membranes were washed (to remove the excess K_2CO_3) and dried in a vacuum oven at 60^oC and -0.1MPa for 24h and stored for characterization.

2.3.2. Synthesis of ECH-CH NFs (ENFs) Membrane

To synthesize ENFs membrane, GNNFs membranes were immersed into 50 mL of 0.01 $mol \cdot L^{-1}$of ECH solution containing 0.067 M (pH 10) of NaOH and agitated for 2 h at 40 °C. After completion of the reaction (Scheme 1), the samples were washed repeatedly with distilled water (to remove the excess ECH) and stored.

2.3.3. Synthesis of Amine grafted (AGNFs) NFs membrane

To synthesize AGNFs membrane, ENFs samples were immersed in 50 mL of DETA solution and agitated for 4 h at 60 °C. The solution of DETA was prepared in 4 $M{\cdot}L^{-1}$ NaOH in 1:10 (e.g.15 mL of DETA with 150 mL of NaOH solution) ratio. After the completion of reaction (Scheme 2), the samples were washed repeatedly with ethanol and distilled water and stored.

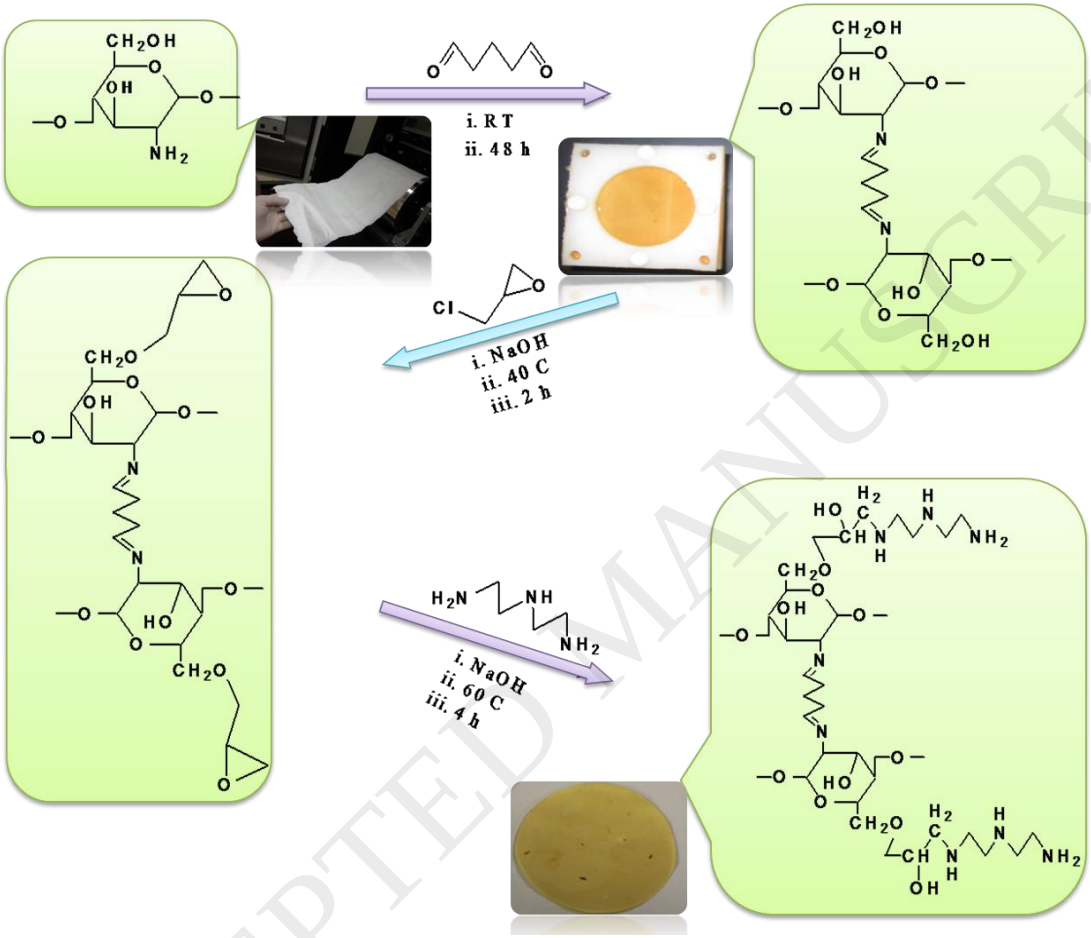

Scheme 2. Novel step wise synthetic route for the synthesis of AGNFs membrane.

2.4. Characterization of the Functionalized NFs Membrane

2.4.1. Morphology Study of the Functionalized NFs

The morphologies of the CHNFs and the functionalized membranes were studied by using a FE-SEM (JSM-7600F). To study the surface morphologies of the membranes *via* FE-SEM, NFs samples were fixed onto a holder with aid of a carbon tape and then placed in the sputtering

machine for platinum coating (to their increase electrical conductivity). After platinum coating the samples were examined by FE-SEM under high vacuum.

2.4.2. FT-IR Study

IR spectra of the CH powder, CH NFs and the functionalized membranes were studied by using FT-IR spectrometer (Bruker Vertex 70). For the FT-IR characterization, the KBr discs of the samples were prepared by mixing and grounding the samples with KBr powder in mortar with a pestle. The mixture was then shaped into discs under mechanical pressure. The samples discs were put into FT-IR and spectral measurements were recorded in the wavenumber range of 800-2200 cm^{-1}. The data was processed by using Software OPUS 6.0 (Bruker), which was baseline corrected by rubber band method with CO_2 and H_2O bands excluded. To further confirm the introduction of the functional group, CHN data was also collected using CHN analyzer.

2.4.3. Stability Study

The degree of stabilities of the NFs and functionalized membranes were studied in distilled water. To measure the degree of stabilities of the mentioned samples, the samples were first completely dried in oven at 100 ^oC for 24 h followed by drying in vacuum oven at 60 ^oC and at -0.1MPa. The dried membrane samples were weighed and their initial weights were recorded manually in a note book. After weighing the samples were immersed in the vial containing distilled water and allowed to remain in the distilled water for different duration of time (1,2, 4, 6, 8, 12, 20 and 24 h) at room temperature. The samples were taken out from the vial at the mentioned time durations, dried (following the same method discussed above) and weighed again. The degree of stability(s) was expressed by the following equation:

$$S\ (\%) = \frac{W1 - W2}{W1} \times 100 \qquad (1)$$

Where W1 and W2 are the initial and final weights of the dried membranes

2.4.4. Thermogravimetric analysis

Thermal behavior of the CH, CH NFs and functionalized NFs membranes was studied using TGA Q50, TA Instruments (United States). Each sample was placed in a platinum plate, weighed and was heated under nitrogen atmosphere at 10 °C/min from 25 to 600 °C.

2.4.5. Adsorption study

Dried samples of the GNF, GNNF and AGNFs mats (0.05 g) were added separately to 10 mL synthetic metal ions solution (400 ppm) and shaked (in a shaker bath (SI-600R)) by a batch technique as a function of time until 24 h at 25 °C. Batch technique is widely used in the adsorption studies for initial ions concentration, pH optimization, and adsorption (Lei Zhang et al; 2016., Doina et al., 2012; Shyam et al., 2014; Md. R. A, 2015). Equilibrium time was determined at 8 h from the saturation point of the adsorption. Adsorption equilibrium isotherm was also studied as a function of the metal-ion concentration at equilibrium time (8h) and 25 °C. The concentration of the metal ions in solution (after adsorption experiment) was determined with an inductively coupled plasma mass spectrophotometer (ICP MS (PerkinElmer) and the amounts adsorbed were calculated as follows:

$$q = \frac{(C_0 - C_f)V}{M} \qquad (2)$$

Where **q** is the amount adsorbed ($mg \cdot g^{-1}$), $\mathbf{C}_0$ and $\mathbf{C}_f$ are the initial and final metal ions concentrations ($mg \cdot L^{-1}$), **V** isqa the solution volume (L) and **M** is the amount of adsorbent (g) used.

3. Results and Discussion

3.1. Morphology study

Figure1 (a-f) shows the FESEM micrographs for CH NFs and functionalized membranes. No significant change in the morphologies of the functionalized NFs membranes was observed.

However, in case of GNNFs, ENF and AGNF, the structure was denser with slightly increased fiber diameter. The dense morphologies of the membranes were attributed to the bonding of GTA, ECH and DETA to the CHNFs. The inset digital image in Fig (b) showed not much crosslinking *via* GTA vapors. This is mainly attributed to presence of ammonium ($-NH_3^+$) ions. The NH_3^+ ions appear in the CH chains, when it is dissolved in TFA solvent. The same membrane when treated with K_2CO_3 in aqueous solution, the color of the membrane became intense (inset Fig (d)). This show that the GTA vapors remained absorbed in the membrane and reacted with NH_2 groups, during the conversion of NH_3^+ ions to NH_2 in neutralization reaction.

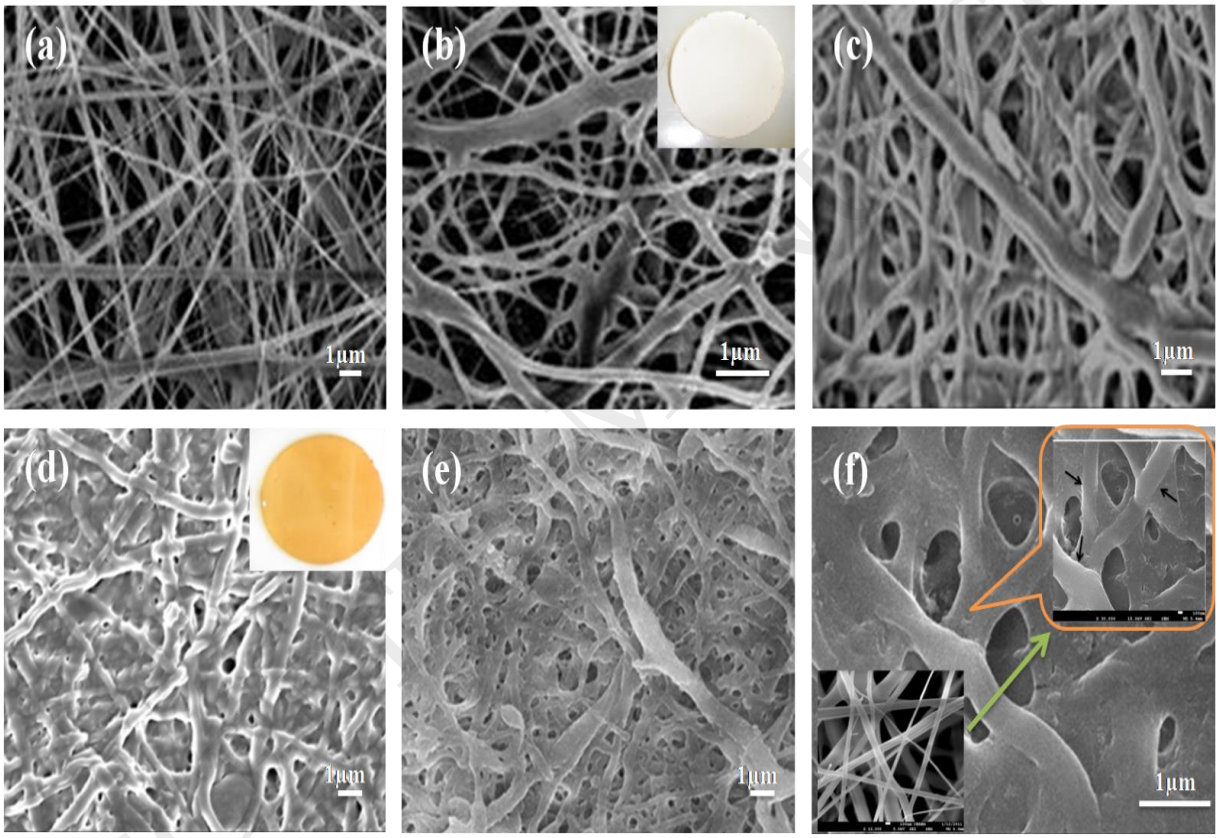

Figure 1**.** FE-SEM micrographs of the surface of the; (a) CH NFs, (b) GNF, (c) NNF (d) GNNF, (e) ENFs and (f) AGNFs membranes.

3.2. FTIR and CHN Studies

FT-IR spectrum is a handy tool to classify molecular functional groups on the basis of their chemical bonds. Chemical bonds usually have unique energies absorption band in the FT-IR

spectrum. Utilizing the knowledge of absorption of bond in the FT-IR spectrum, we can obtain structural and bonding information. Figure 2 shows the FT-IR spectra of the CH NFs and functionalized NFs membranes. The FTIR spectra of CH showed typical scissor vibration band of amine ($-NH_2$) at 1630 cm^{-1} and carbonyl group (C=O) stretching band of the N-acetyl at 1680 cm^{-1}.The NF membrane exhibited sufficient decrease in scissor vibration band of amine (at1630 cm^{-1}), increase in the intensity of C=O stretching band due the increased C=O concentration of trifluoroacetate ($CF3COO^-$) ions and a new band for ammonium ($-NH_3^+$) ion at 1538 cm^{-1} (Haider et al., 2008). The $-NH_3^+$ ion band appeared in the NFs membrane as result of the salt formation between $-NH_3^+$ and acetate ($-COO^-$) ions, when CH powder is dissolved in TFA. The formation of salt between $-NH_3^+$ and–COO^- ions has been reported in the literature (Haider and Park, 2009; Sangsanoh and Supaphol, 2006; Mincheva et al., 2004). In the GNF membrane, the shoulder scissor vibration band of amine at 1630 cm^{-1} further decreased and the intensity of the C=O stretching band at 1680 cm^{-1}, primarily assigned to N-acetyl, is increased (augmented) (Ke et al., 2011). This increase in intensity was attributed to the overlapping of C=O and C=N (imine) stretching bands. The imine formation (aldol type of reaction) between free amino and aldehyde group of GTA has been reported in the literature (Schiffman and Schauer, 2007). The FT-IR data is supported by the digital images in Scheme 2. The appearance of yellow color is attributed to the formation of imine (C=N) (Haider et al., 2010; Zhang et al., 2006). The GNNF membrane showed only scissor vibration band of amine (($-NH_2$) at 1630 cm^{-1}. The $-NH_3^+$ ion band at 1538 cm^{-1} disappeared completely, which supported our above discussion in favor of functionalization. Functionalization was found more prominent in GNNF sample as compared to CH NF sample because more $-NH_2$ were available in GNNF as compared to CH NF membrane. The ENF membrane showed a band between 1000 and 1200 cm^{-1} with an increased intensity whereas the rest remain at their positions. The increased intensity of the band between 1000 and 1200 cm^{-1} (Liu et al., 2011) indicated the formation of C–O bond between ECH and CH during the reaction. This peak might also be attributed to the

C–O–C stretching of cyclic ether, which suggested that cyclic structure of epoxy is preserved (scheme 1) during the reaction (Socrates, 2001). The grafting reaction of amine group proceeded *via* ring opening of the terminal epoxy. AGNFs membrane showed considerable decrease in the peak between 1000-1200 cm^{-1}. This decreased intensity might be attributed to the ring opening (Scheme1) of the cyclic epoxy (Socrates, 2001). The increased intensity is observed for small ring size between 1000-1200 cm^{-1}. The band at 1630 $cm^{-1}$for primary amine became broader and slightly reduced. The broadness and slight reduction in the intensity might be due to two effecting factors: first, the absorption of primary amine due to N-H deformation is medium to strong in this region (Lewandowska, 2009) and second the overlapping of carbonyl (C=O) and imine (C=N) stretching bands. Secondary amine (CH-NH-CH) on the other hand showed a weak peak (due to N-H deformation) in the region of 1400-1500 cm^{-1}. The above discussion is further supported by the CHN data (Table 2) where significant increase in the Carbon, Hydrogen and Nitrogen for the AGNFs was observed. The complementation of FTIR (Figure 2) by CHN data (Table 2) strongly suggests that our desired product is formed.

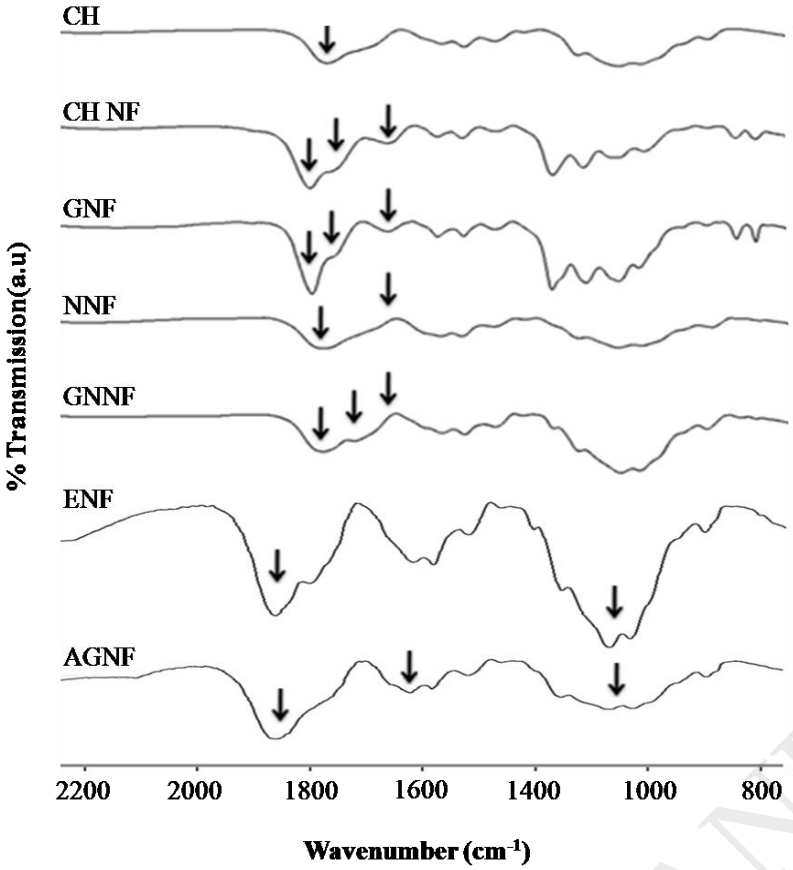

Figure 2. FTIR spectra of the CH NFs and functionalized NFs membranes.

Table 2. CHN data for the functionalized NFs membrane.

Compound	**% Found**			**Total**
	C	H	N	
NF	33.84	5.19	5.37	44.4
GNNF	36.90	5.41	5.21	47.52
ENF	39.49	6.49	6.45	52.43
AGNF	43.23	7.32	7.30	57.85

3.3. Stability Study

Figure 3 shows the degree of stability (calculated according to Eq. (1)) of the GNF, NNF, GNNF, ENF and AGNF membranes in distilled water. CH NF got dissolved as soon it was

immersed in the vial. The reason for this dissolution was the salt formation between the -NH_3^+) and–COO^- ions (discussed in detail FT-IR Study). GNF, NNF, GNNF, ENF and AGNF samples showed various degree of stability in the distilled water. The order of stability until 24 h was: NNF (97% weight remained), ENF (96% weight remained), GNNF and AGNF (94% weight remained) and GNF (66% weight remained). NNF, ENF, GNNF and AGNF membranes showed good stability as compared to GNF. This high stability might be due to the complete conversion of the salt of -NH_3^+ and –COO^- ions in to amine -NH_2 (in case of NNF), formation of imine (C=N) (in case of GNNF, ENF and AGNF) and least formation of imine (C=N), (in case of GNF). This fact is also evident from the intense yellow color in Figure 1d and the marginal yellow color in Figure 1b.

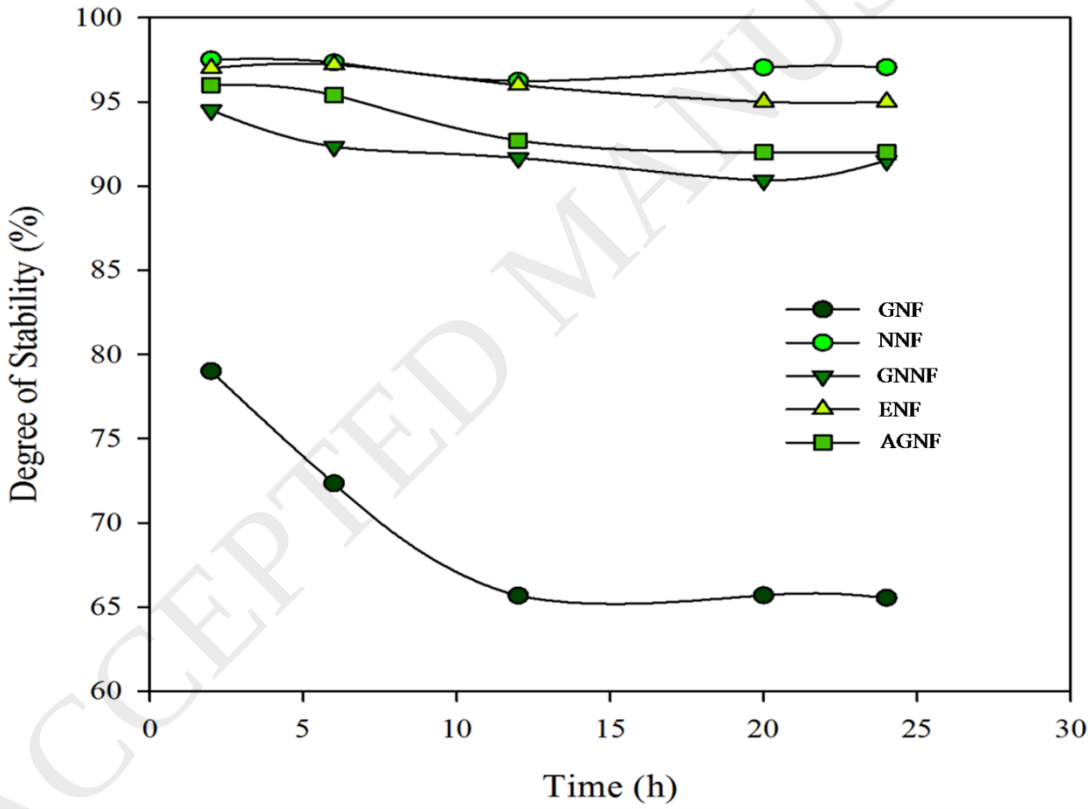

Figure 3. Degree of stability of the functionalized NFs membranes in distilled water.

3.4. Thermogravimetric analysis

Figure 4 shows thermal behavior of CH, CHNF, GNF, GNNF, ENF and AGNF membranes. In the thermogram of the CH, the weight loss occurred in two stages: the initial weight loss

occurred in the region of 30-100 ºC, which is attributed to moisture evaporation and the second weight loss occurred in the region of 260-333 ºC due to the degradation of the polysaccharide chains and dehydration of deacetylated units (Lewandowska, 2009). The weight loss at 333 ºC was 52%. CH NF and GNF membranes showed similar patterns. These membranes were decomposed in the region of 130-333 ºC and the weight loss was 75%. This increased weight loss might be due to the presence of TFA (Qi et al., 2008) and added GTA, which induced thermal degradation. The GNNF membrane was thermally decomposed at 230-333ºC. The ENF and AGNF membranes were decomposed in two regions: first in the region of 30-130ºC in case of ENF and 30-150ºC in case of AGNF, and second in the region of 190-600ºC in case of ENF and 220-600 ºC in case of ENF. The weight loss in the first region could be attributed to the evaporation of moisture (until 100 ºC) and the added organics (above 100 ºC). The weight loss for the AGNF was 48%. From the above discussion we have concluded that GNNF, ENF and AGNF were thermally more stable as compared to CH NF and GNF. This fact might be attributed to the increase bonding density in GNNF, ENF and AGNF, which has resulted in more compact chemical structures.

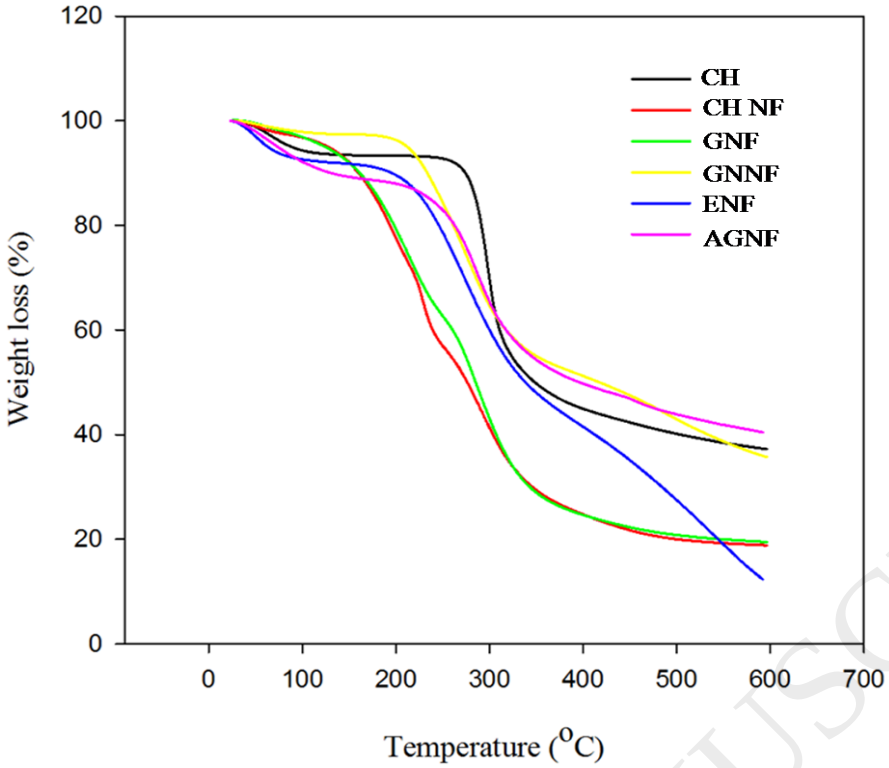

Figure 4. TGA thermograms for CH, NF and functionalized NFs membranes.

3.5. Adsorption Kinetics and Isotherms

Increase in the metal ions pollutions of water resources with industrialization has generated great concern in the last decade. Metal ions are not only toxic to human beings but also to animals and plants at very low concentrations. A number of papers have been published on the performance of processed and functionalized CH for the removal metal ion. However, very few have shown efficient results. We have combined the processing and functionalization of CH and studied their effect on the removal of metal ions from aqueous solution. Figure.5a shows the adsorption of kinetics of Cu(II) and Pb(II) ions onto the functionalized CH NFs membrane (in a 400 ppm synthetic solutions) was studied as a function of time. The adsorption for both metals ions increased sharply from 30 min to 6 h and then leveled off at 8 h. The shape of the curve indicated that the binding of metal ions to the chelating sites on the adsorbent increased sharply upto 6 h and was homogeneously saturated after 8 h (Haider and Park, 2009). This fact is supported by Langmuir model in the adsorption isotherm study {Yu Liu et al., 2008; Md, R.

A et al., 2014). Figure5b and Figure5c shows the equilibrium adsorption amounts of Cu(II) and Pb (II) ions onto functionalized NFs membrane at equilibrium time (8 h, determined from Figure.5a) as function of equilibrium concentrations. The adsorption of both the Pb(II) and Cu(II) ions increased rapidly with increase in the initial concentration, however, further increase in the concentration led to a gradual decrease in the adsorption. The initial increase might be attributed to the increased surface area (due to nano size) and easily available binding sites (such as amine, primary and secondary hydroxyl groups). The decrease is, however, attributed to the saturation of the binding sites and competition between the ions to occupy these sites. To have a further insight into the adsorption phenomena, the adsorption equilibrium data of Cu(II) and Pb(II) ions were analyzed with the following Langmuir adsorption equation

$$\frac{C_e}{q_e} = \frac{1}{K_L q_m} + \frac{C_e}{q_m} \qquad (3)$$

where q_e, is the equilibrium quantity of the metals ions adsorbed onto the CH NFs mat (mg. g^{-1}), C_e is the equilibrium concentration (mg. L^{-1}), and q_m (mg. g^{-1}), and K_L (L.mg^{-1}) are the Langmuir constants related to the saturation adsorption capacity and binding energy (affinity), respectively (Yu and Hui, 2007; Yu Liu et al., 2008).

Figure.5d and 5e shows the Langmuir C_e/q_e versus C_e plots for Cu(II) and Pb(II) ions, Good linear relationship (r^2 were over 0.99) was found for both metal ions. This could be explained on the basis of Langmuir theory, which states that adsorption takes place at specific homogeneous sites within the adsorbent (Haider and Park, 2009; Yu Liu et al., 2009; Md. R. A et al., 2016; Md. R. A et al., 2016; Md. R. A et al., 2013; Md. R. A et al., 2013). Thus, monolayer adsorption occurs on all the NF membranes. Table 3 shows the values of q_m and K_L, which were calculated from the slope and intercept of the C_e/q_e versus C_e plots. Increased maximum adsorption (q_m) capacities were observed for GNNF (90.90 mg.g^{-1}, Pb(II) and 158.73, Cu (II)) and AGNF (94.34 mg.g^{-1} for Pb(II) and 166.67 for Cu(II)). This increase is attributed to the availability of the increased number of amine binding sites (nitrogen which

donates lone-pair of electron for chelation). Whereas the decrease in q_m for ENF (84.03 $mg.g^{-1}$ for Pb(II) and 151.52 for Cu(II)) membrane might be correlated to the increase in the hydrophobic chain (carbon atom), no amine bind sites (nitrogen was occupied), decrease in the oxygen binding sites and increased bonding density resulting in a compact structure. The adsorption capacity of the present systems was much higher, particularly for Cu(II) when compared to conventionally processed CH and other adsorbents (Table 4) (Helder et al, 2007; Justus et al, 2004; Ngah et al., 2002; Bassi et al., 2000; Huang et al., 1996). The adsorption and desorption experiments were via batch techniques for 3 cycles (Figure 6). The data obtained from the experiments showed that desorption capacity dropped as compared to the first cycle which can be attributed to the decomposition or damage caused by acidic solution to certain adsorption sites or functional groups present over the nanofibers membrane.

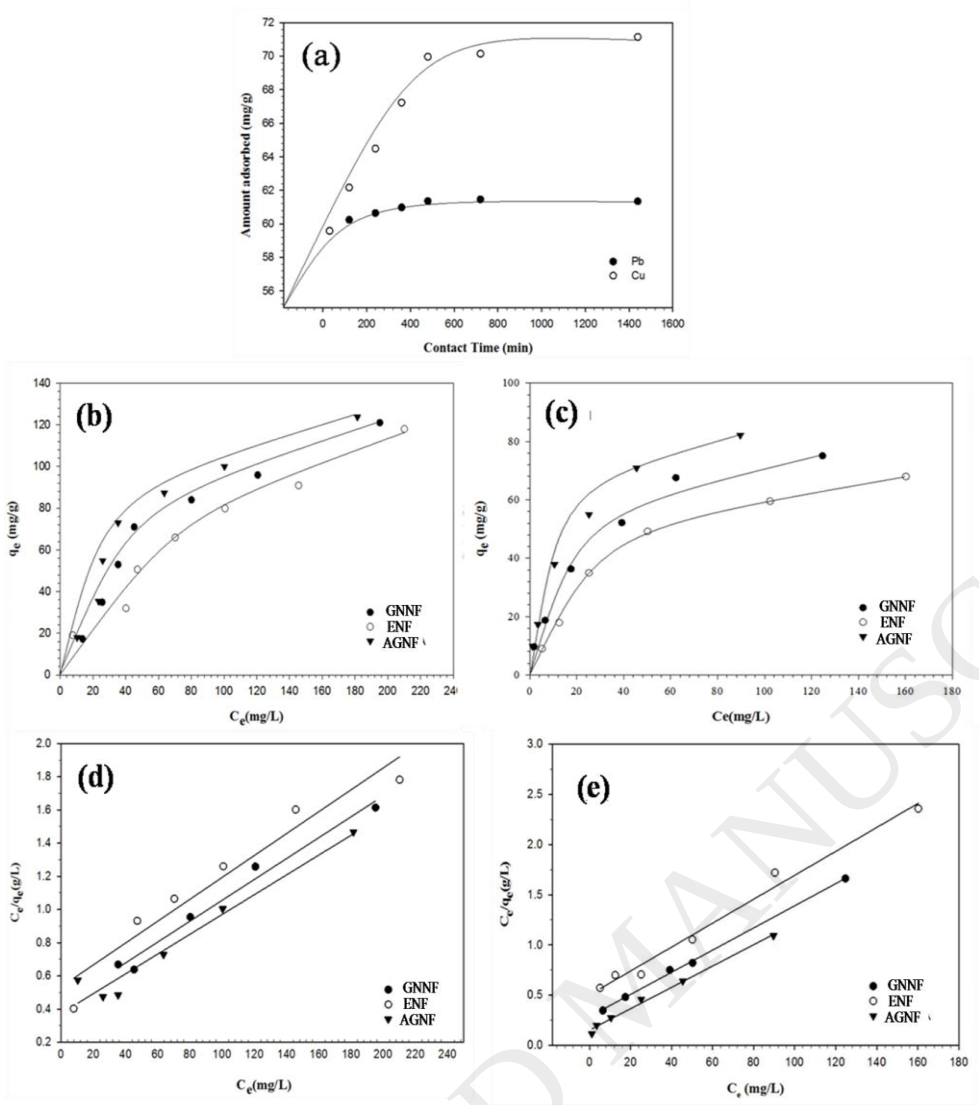

Figure 5. Adsorption kinetics and isotherms on to functionalized NFs membranes; (a) adsorption kinetics of Pb(II) and Cu(II), (b-c) adsorption isotherm of Cu(II) and Pb(II), (d-e) Langmuir model isotherm of Cu(II) and (e) Pb (II). The experiments were performed in tirpilcate. The Data had a standard deviation of +_ 0.05.

Table 3. Langmuir adsorption constants.

	Cu(II)			Pb(II)		
Functionality	**q_m ($mg.g^{-1}$)**	**K_L ($L.mg^{-1}$)**	**r^2**	**q_m ($mg.g^{-1}$)**	**K_L ($L.mg^{-1}$)**	**r^2**
GNNF	158.73	2.34	0.9902	90.90	3.42	0.9993
ENF	151.52	1.87	0.9669	84.03	1.98	0.9927

AGNF	166.67	2.67	0.9770	94.34	6.52	0.9967

Table 4. Comparsion of the maxium adsorption capacities (q_m) of various adsorbents from literature and the present work(*).

Adsorbent	**Cu(II) q_m (mg.g^{-1})**	**Adsorbent**	**Pb(II) q_m (mg.g^{-1})**
Anaerobically digested sludge (Gould and Genetelli, 1978)	49.00	Chitosan flakes (Bassi et al., 2000)	12.61
Calculium-aliginate (Huang et al., (1996)	15.80	Sphagnum moss peat (Allen et al, 1992)	61.80
Activated sludge (Gupta,1998)	35.30	Banana stem (Noeline et al., 2005)	91.74
Chitosan (Plain) (Huang et al., 1996) and chitosan flakes (Bassi et al., 2000)	45.20 - 2.83 & 20.92	Tea leaves (Tee and Khan, 1998)	71.80
Chitosan microsphere (Ngah et al., 2002)	80.70, 39.10	Montmorillonite clay (Farrah et al., 1980)	71.80
Chitosan modified with reactive blue (Helder et al., 2007)	57.00	XAD-4Copolymer resin (Ekin et al., 2004)	12.20
Chitosan crosslinked with ether diglycidyl-ethylene glycol (Ngah etal., 2002)	49.90	Polyethylene glycol/chitosan (Wang and Kuo, 2007)	185.00
Chitosan crosslinked with glutaraldehyde (Ngah et al., 2002)	59. 70	Polyethyleneimine (Smith et al., 1996)	120.00
Chitosan crosslinked with epichloridrine (Ngah et al., 2002)	62.50	PEO/Chitosan nanofibers (Abadi et al., 2013)	237.20
Chitosan modified with 2 [-bis-(pyridylmethyl) aminomethyl]-4 methyl-6-formyl-phenol (Justus et al., 2004)	109.00	SCBA(Salihi et al., 2017)	23.40
*****Amine grafted chitosan nanofibers (AGNFs)	*****166.67	Amine grafted chitosan nanofibers (AGNFs)	94.34
Mesoposous conjugate materials (Md. Rabiul Awual et al., 2016)	174.76	Ligand based conjugate (Md. Rabiul Awual et al., 2014)	195.31
Mesoporous Silica composite (Md. Rabiul Awual et al., 2015)	200.80		
Mesoporous adsorbent (Md. Rabiul Awual et al., 2014)	182.39	Mesoporous adsorbent (Md. Rabiul Awual et al., 2014)	172.53

*** Note. Present work**

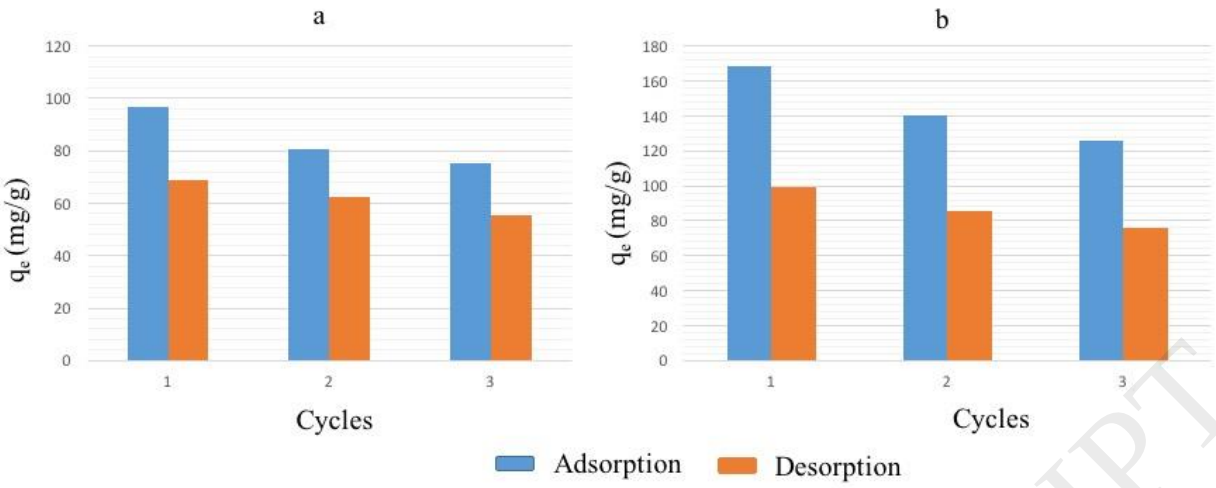

Figure 6. Adsorption-desorption and regeneration studies of functionalized NFs membranes,(a) Pb(II) ions and (b) Cu(II)ions. The experiments were performed in tirpilcate. The Data had a standard deviation of +_ 0.05.

4. Conclusion

The novel step wise synthetic route was developed to prepare AGNFs membrane. FT-IR and CHN data confirmed the introduction of new functional groups into the primary structure of CH. FE-SEM micrograph showed no deterioration of the CH NFs morphology after grafting. The AGNFs membranes showed good aqueous stabilities (with only ~6% loss in weight until 24 h) which was less than the weight loss by GNF (~44% loss in weight until 24 h) and CH NFs (100% loss in weight as soon as it was immersed in distilled water). The maximum adsorption (q_m) capacities of AGNFs for Cu (II) and Pb (II) were observed to be 166.67 $mg.g^{-1}$ and 94.34 $mg.g^{-1}$. The adsorption capacity of the present systems was much higher for Cu (II) when compared to the already existing conventional and CH adsorbents. This increased could be attributed to not just to the nano-size, but more potentially to the increase in the number of nitrogen binding sites (chelating sites; nitrogen donates lone-pair of electron for chelation). The combination of CH processing to NF and amine grafting has significantly increased the adsorption capacity of CH NFs membranes.

Acknowledgement

One of the author (Sajjad Haider) would like to extend his sincere appreciation to the Deanship of Scientific Research (DSR) at King Saud University for its funding of this research through the Research Group no RG-1437-029.

5. Reference

Abadi, M.A. Irani, M., Ismaeili, Piri, J. H. Parnian, M.J. (2013). Electrospun nanofiber membrane of PEO/Chitosan for the adsorption of nickel, cadmium, lead and copper ions from aqueous solution. Chemical Engineering Journal 220, 237-243.

Ahmed, S., Md, R. A., Md, A. K., Md, Z. A., Sarwaruddin C.A.M., (2015). Large-pore diameter nano-adsorbent and its application for rapid lead(II) detection and removal from aqueous media, Chemical Engineering Journal, 273 286-295

Allen, S. Brown, P. McKay, G. Flynn, O. (1992). An evaluation of single resistance transfer models in the sorption of metal ions by peat. Journal of Chemical Technology and Biotechnology 54 (3) 271–276

Bassi, R. Prasher, S.O. Simpson, B.K. (2000). Removal of selected metals ions from aqueous solutions using chitosan flakes Separation Science and Technology 35 (4), 547–560.

Burger, C. Hsiao, B. Chu, S B. (2006). Nanofibers materials and their applications. Annual Review of Materials Research 36 333-368.

Crini, G. Badot, P.-M. (2008). Applications of chitosan a Natural aminopolysaccharide for dye removal from aqueous solutions by adsorption processes using batch studies: A review of recent literature. Progress in Polymers Science 33 (4) 399-447.

Doina, H., Gianina, D, Marcel, I. P, (2012). Heavy Metal Ions Adsorption on Chitosan-Magnetite Microspheres, International Review of Chemical Engineering Vol. 4 (3) 364-368.

Ekic, S.D. Filik, C. H. Apak, R. (2004). Use of an o-aminobenzoic acid-functionalized XAD4 copolymer resin for the separation and preconcentration of heavy metal (II) ions. Analytica Chimica Acta 505 (1) 15–24.

Farrah, H. Hatton, D. Pickering, W.F. (1980). The affinity of metal ions for clay surfaces. Chemical Geology 28, 55–68.

Gould, M.S. Genetelli, E.J. (1978). Heavy metals complexation anaerobically digested sludge Water Research. 12 (8), p. 505-512.

Gupta,V.K. (1998). Equilibrium uptake, sorption dynamics, process development, and column operations for removal of copper and nickel from aqueous solution ad wastewater using activated slag, a low cost-cost adsorbent Indian and Engineering Chemistry Research 37 (1), 192–202.

Haider, S. Al-Zeghayer, Y .S. Al-Masry, W.A. Ali, F.A.A. (2012). Fabrication of chitosan nanofibers membrane with improved stability and britility Advance Science Letters 17 (1), 217-223.

Haider, S. Al-Masry, W. A. Bukhari, N. Javid, M. (2010). Preparation of the chitosan containing nanofibers by electrospining chitosan gelatin complexes. Polymer Engineering and Science 50 (9) 1887-1893

Haider, S. Park, S.Y. (2009). Preparation of the electrospun chitosan nanofibers and their applications to the adsorption of Cu (II) and Pb (II) ions from an aqueous solution. Journal of Membrane Science 328 (1) 90-96.

Haider, S. Park, S.Y. Lee, S.H. (2008). Preparation, swelling and electro mechano chemical behaviours of a gelatin chitosan blend membrane Soft Matter 4 (3) 485-49

Helder, L.V. Valfredo, T.F. Norberto, S.G. Mauro, C.M.L. (2007). Chitosan modified with reactive blue 2 dye on adsorption equilibrium of Cu (II) and Ni (II) ions Reactive and Functional Polymers 67 (10) 1052–1060.

Huang, Z. M. Zhang, Y. Kotaki, Z. M. Ramakrishna, S. (2003). A review on polymer nanofibers by electrospining and their applications in nanocomposites. Composite Science Technology 63 2223-2253.

Huang, C. Chung, Y.C. Liou, M.R. (1996). Adsorption of Cu (II) and Ni (II) by pelletized biopolymer Journal of Hazardous Materials 45 (2-3), 265–277.

Justus, K.C. Laranjeiraa, M.C.M. Nevesa, A. Mangrich, A.S. Fáverea, V.T. (2004). Chitosan functionalized with 2[-bis-(pyridymethyl) aminomethyl]4-methyle-6-formyl-phenol: Equilibrium and kinectics of copper (II) adsorption Polymer, 45 (18), 6285-6290.

Katti, D. S. Robinson, K. W. Ko, F. K. Laurencin, C. T. (2004). Bioresorbable nanofiber-based systems for wound healing and drug delivery: optimization of fabrication parameters. Journal of Biomed Materials Research Part B 70 (2) (286-296.

Ke, W.Z. Ling, H.U. Q. Xiang, W. Y. (2011). Preparation of chitosan rods with excellent mechanical properties: one candidate for bone fracture internal fixation. Science China Chemistry 54 (2) 380-384.

Kotaki, Z. Ma, M., Inai, R., and Ramakrishna, S. (2005). Potential application of nanofiber matrix as tissue-engineering scaffolds. Tissue Engineering 11(1-2) 101-109.

Kim, G. M., Michler. H., Potschke, P. (2005). Deformation process of ultrahigh porous carbon nanotube/polycarbonate composite fiber prepared by electrospining. Polymer, 46 (18) 7346-7351.

Lewandowska, K. (2009). Miscibility and thermal stability of poly(vinyl alcohol) chitosan mixture. Thermochimica Acta 493 (1-2) 42-48.

Lei, Z., Yuexian, Z., Zhengjun, C., (2016). Removal of heavy metal ions using chitosan and modified chitosan: A review. Journal of Molecular Liquids Volume 214, 175-191

Liu, Y. Liu, Y. Cao, X. Hua, Wang, R. Pang, Y. Hua, C. M. Li, X. (2011). Biosorption studies of uranium (IV) on cross linked chitosan: isotherm kinectics and thermodynamic aspect. Journal of Radioanalytical and Nuclear Chemistry, 290 (2), 231-239.

Ma, Z., Kotaki, M., Ramakrishna, S. (2005). Electrospun cellulose nanofiber as affinity membrane. Journal of Membrane Science, 265 (1-2), 115-123.

Md, R. A., Tsuyoshi, Y., El-Safty, A.S., Hideaki, S., Yoshihiro, O., (2013) Copper(II) ions capturing from water using ligand modified a new type mesoporous adsorbent, Chemical Engineering Journal, 221 322-330

Md, R. A., Mohamed, I., Tsuyoshi, Y., El-Safty, S. A., Shinichi, S., (2013) Trace copper(II) ions detection and removal from water using novel ligand modified composite adsorbent, Chemical Engineering Journal, 222 67-76

Md, R. A., Md, M. H., (2014) Novel conjugate adsorbent for visual detection and removal of toxic lead(II) ions from water, Microporous and Mesoporous Materials, 196, 261-269.

Md, R. A., Ismail, M.M. R., Tsuyoshi, Y., Md, K., Ferdows, M. (2014). pH dependent Cu(II) and Pd(II) ions detection and removal from aqueous media by an efficient mesoporous adsorbent, Chemical Engineering Journal, 236, 100-109.

Md, R. A., Muhammad, I., (2014). Efficient gold (III) detection, separation and recovery from urban mining waste using a facial conjugate adsorbent, Sensors and Actuators B: Chemical 196, 457-466.

Md, R. A., Md, M. H., Ahmed, S., (2014). Functionalized novel mesoporous adsorbent for selective lead(II) ions monitoring and removal from wastewater, Sensors and Actuators B: Chemical, 203 854-863.

Md, R. A., Md, M. H., (2014). A novel fine-tuning mesoporous adsorbent for simultaneous lead(II) detection and removal from wastewater, Sensors and Actuators B: Chemical, 202 395-403.

Md, R. A., Md, M. H., (2015). Colorimetric detection and removal of copper(II) ions from wastewater samples using tailor-made composite adsorbent, Sensors and Actuators B: Chemical, 206, 692-700.

Md, R. A., Md, M. H., Mu, N., Hideaki, S., Tsuyoshi, Y., (2015). Preparation of new class composite adsorbent for enhanced palladium (II) detection and recovery, Sensors and Actuators B: Chemical, 209 790-797.

Md, R. A., Md, A. K., Yeasmin, R., Hussein, Z., (2015). Simultaneous ultra-trace palladium(II) detection and recovery from wastewater using new class meso-adsorbent, Journal of Industrial and Engineering Chemistry, 21 405-413.

Md, R. A., (2015). A novel facial composite adsorbent for enhanced copper(II) detection and removal from wastewater, Chemical Engineering Journal, 266 368-375

Md, R. A., Md. M. Hasan, Md. A. Khaleque, Md. C. S. (2016). Treatment of copper(II) containing wastewater by a newly developed ligand based facial conjugate materials. Chemical Engineering Journal, 288, 368-376

Md, R. A., (2016). Solid phase sensitive palladium (II) ions detection and recovery using ligand based efficient conjugate nanomaterials, Chemical Engineering Journal, 300 264-272

Md, R. A, (2016). Ring size dependent crown ether based mesoporous adsorbent for high cesium adsorption from waste water, Chemical engineering journal, 303 539-546.

Md, R. A., (2016). Assessing of lead (III) capturing from contaminated wastewater using ligand doped conjugate adsorbent, Chemical Engineering Journal, 289 65-73

Md, R. A., (2017). Novel nanocomposite materials for efficient and selective mercury ions capturing from waste water, Chemical Engineering Journal, 307 456-465

Md, R. A., (2017). New type mesoporous conjugate material for selective optical copper (II) ions monitoring and removal from polluted waters, Chemical Engineering Journal, 307 (2017) 85-94

Md, R. A., Majeda, K., Nabeel, H. Alharthi, Monis, L., Md, A. K., (2018). Efficient detection and adsorption of cadmium (II) ions using innovative nano-composite materials, Chemical Engineering Journal, 343 118-127.

Mourya, V.K. Inamdar, N. N. (2008). Chitosan modification and applications: opportunity galore. Reactive and functional polymers 68 (6) 1013-1051.

Mincheva, R. Manolova, Sabov, N. R. and Kjurkchiev, G. Rashkov, I. (2004). Preparation of chitosan containing nanofibers by electrospining of chitosan/poly (ethylene oxide) blend solutions. e-Polymers 4 (1), 1–1

Noeline, B.F. Manohar, D.M. Anirudhan, T.S. (2005). Kinetic and equilibrium modeling of lead (II) sorption from water and wastewater by polymerized banana stem in a batch reactor. Separation and Purification Technology 45 (2) 131–140.

Ngah, W.S. Endud, C.S. Mayanar, R. (2002) Removal of copper (II) ions from aqueous solution and cross-linked chitosan beads Reactive Functional Polymers 50 (2), 181-190.

Qi, L. Pal, S. Dutta, P. Seehra, M. Pei, M. (2008). Morphology controllable nanostructured chitosan matrix and its cytocompatibility. Journal of Biomedical Materials Research A 87 (1) 236-244.

Salihi, I. U. Kutty, S.R.M, Isa, M. H. (2017). Adsorption of Lead ions onto Activated Carbon derived from Sugarcane bagasse, IOP Conf. Series: Materials Science and Engineering 20 012034

Saeed, K., Haider, S, Oh, T.J., Park, S.Y. (2008). Preparation of amidoxime-modified polyacrylonitril (PAN-Oxime) nanofibers and their applications to metal ions adsorption. Journal of Membrane Science, 322 (2), 400-405.

Sangsanoh, P. Supaphol, P. (2006). Stability improvement of electrospun chitosan nanofibrous membranes in neutral or weak basic aqueous solutions. Biomacromolecules 7 (10) 2710-2714.

Schiffman, J. D. Schauer, C. L. (2007). Cross linking chitosan nanofibers. Biomacromolecules 8 (2) 594-601.

Shyam, R., Khairkar, A., Raut, R., (2014). Adsorption studies for the removal heavy metal by chitosan-g-poly (acrylicacid-co-acrylamide) composite, Science Journal of Analytical Chemistry 2 (6) 67-70.

Smith, B.F. Robison, T.W. Sauer, N.N. Ehler, D.S. Water-soluble polymers for recovery of metals from soils, sludges, or wastes, US Patent 5,928,517 (1996).

Socrates, G. Infrared and Raman Characteristic Group Frequency. 3rd edition, publisher John Wiley and Sons, 2001, p 102-108.

Tee, T.W. Khan, A.R.M. (1988). Removal of lead, cadmium and zinc by waste tea leaves. Environmental Technology Letters. 9 (11) 1223–1232.

Ueno, H. Mori, T. Fujinaga, T. (2001). Topical formulations and wound healing applications of chitosan. Advance Drug Delivery Review 52 (2) 105-115.

Wang, H.S. Fu, G-D. Li, X-S. (2009). Functional polymeric nanofibers from electrospining. Recent Patents on Nanotechnology 3 (1) 21-31.

Wang, J.W. Kuo, Y.M. (2007). Preparation of fructose-mediated (polyethylene glycol/chitosan(membrane and adsorption of heavy metal ions. Journal of Applied Polymer Science 105 (3) 1480–1489.

Yu, L., Hui, X., (2007). Equilibrium, thermodynamics and mechanisms of Ni2+ biosorption by aerobic granules, Biochemical Engineering Journal 35 (2) 174-182.

Yu, L., Ya-Juan, L., (2008). Biosorption isotherms, kinetics and thermodynamics, Separation and Purification Technology 61(3) 229-242).

Yu, L., (2009) Is the Free Energy Change of Adsorption Correctly Calculated? Journal of Chemical Engineering Data 2009, 54 (7) 1981-85.

Zhang, H. Li, S. White, C. J. B. Ning, X. Nie, H. Zhu, L. (2009). Studies on electrospun nylon 6/chitosan nanofibers interactions. Electrochimica Acta 54 (24) 5739-5745.

Zhang, Y. Venugopal, Z. J. Huang, Z.-M. Lim, C.T. Ramakrishna, S. (2006). Crosslinking of the electrospun gelatin nanofibers. Polymer 47 (8) 2911-2917.